Hydrol. Earth Syst. Sci. Discuss., https://doi.org/10.5194/hess-2018-200
Manuscript under review for journal Hydrol. Earth Syst. Sci.
Discussion started: 23 April 2018

Hydrology and Earth System Sciences
Discussions
Open Access

Hydrological effects of climate variability and vegetation dynamics on annual fluvial water balance at global large river basins

Corresponding author:

Qiang Zhang, Ph.D. Professor, Associate editor of HSJ and JH

Key Laboratory of Environmental Changes and Natural Hazards, Ministry of Education, Academy of Hazard Reduction and Emergency Management, & State Key Laboratory of Earth Surface Processes and Resource Ecology

Beijing Normal University

Beijing 100875,

China.

Tel: +86-10-58807086

E-mail: zhangq68@bnu.edu.cn (preferred contact address)

Hydrol. Earth Syst. Sci. Discuss., https://doi.org/10.5194/hess-2018-200
Manuscript under review for journal Hydrol. Earth Syst. Sci.
Discussion started: 23 April 2018

Hydrology and Earth System Sciences
Open Access
Discussions

Jianyu Liu[1], Qiang Zhang[2,3*], Vijay P. Singh[4], Changqing Song[2,3], Yongqiang Zhang[5], Peng Sun[6]

[1]Laboratory of Critical Zone Evolution, School of Earth Sciences, China University of Geosciences, Wuhan 430074, China

[2]Key Laboratory of Environmental Change and Natural Disaster, Ministry of Education, Beijing Normal University, Beijing 100875, China

[3]Faculty of Geographical Science, Academy of Disaster Reduction and Emergency Management, Beijing Normal University, Beijing 100875, China

[4]Department of Biological and Agricultural Engineering and Zachry Department of Civil Engineering, Texas A&M University, College Station, Texas, USA

[5]CSIRO Land and Water, GPO Box 1700, Canberra ACT 2601, Australia

[6]College of Geography and Tourism, Anhui Normal University, Anhui 241000, China

Hydrol. Earth Syst. Sci. Discuss., https://doi.org/10.5194/hess-2018-200
Manuscript under review for journal Hydrol. Earth Syst. Sci.
Discussion started: 23 April 2018

Hydrology and Earth System Sciences
Open Access
Discussions

Abstract: The partitioning of water and energy, governed by the controlling parameter in the Budyko framework (i.e., *n* parameter in the Choudhury and Yang equation), is critical to assess the water balance at global scale. It is widely acknowledged that the spatial variation of this controlling parameter is affected by landscape characteristics, but characterizing its temporal variation remains yet to be done. Considering effective precipitation (P_e), the Budyko framework was extended to the annual water balance analysis. To reflect the mismatch between water supply (precipitation, P) and energy (potential evapotranspiration, E_0), a climate seasonality and asynchrony index (SAI) were proposed in terms of both phase and amplitude mismatch between P and E_0. Considering streamflow changes in 26 large river basins as a case study, SAI was found to the key factor explaining 46% of the annual variance of parameter n. Furthermore, the vegetation dynamics (M) remarkably impacted the temporal variation of n, explaining 67% of the variance. With SAI and M, a semi-empirical formula for parameter n was developed at the annual scale to describe annual runoff (R) and evapotranspiration (E). The impacts of climate variability (P_e, E_0 and SAI) and M on R and E changes were then quantified. Results showed that R and E changes were controlled mainly by the P_e variations in most river basins over the globe, while SAI acted as the controlling factor modifying R and E changes in the East Asian subtropical monsoon zone, E_0 in the temperate maritime climate of Europe, and M in the temperate grassland zone of South America.

1. Introduction

Climate variability, vegetation dynamics and water balance are interactive, and this interaction is critical in the evaluation of the impact of climate change and vegetation dynamics on water

Hydrol. Earth Syst. Sci. Discuss., https://doi.org/10.5194/hess-2018-200
Manuscript under review for journal Hydrol. Earth Syst. Sci.
Discussion started: 23 April 2018

Hydrology and Earth System Sciences
Open Access
Discussions

balance at the basin scale and for the management of water resources (Milly, 1994; Yang et al., 2009; Weiss et al., 2014; Zhang et al., 2016c). The models that can quantify the climate-vegetation-hydrology interactions without calibration using observed evapotranspiration/runoff are particularly needed for hydrological prediction in ungauged basins (Potter et al., 2005). Furthermore, quantifying the influence of climate variability and vegetation dynamics on hydrological variability is critical in differentiating the factors that drive the hydrological cycle in both space and time (Yan et al., 2014; Dagon and Schrag, 2016; Zhang et al., 2016a).

The Budyko framework was developed to quantify the partitioning of precipitation into runoff and evapotranspiration (Koster and Suarez, 1999; Xu et al., 2013), and was widely used to evaluate interactions amongst climate, catchment characteristics, and hydrological cycle (Yang et al., 2009; Cai et al., 2014; Liu et al., 2017b; Ning et al., 2017). However, the controlling parameter of the Budyko framework usually needs to be calibrated, based on observed data. If the controlling parameter can be determined using the available data, then the Budyko framework can be employed in modelling the hydrological cycle in ungauged basins (Li et al., 2013). That is why considerable attention has been devoted to quantifying the relationship between the controlling parameter and explanatory variables (e.g. Yang et al., 2009; Abatzoglou and Ficklin, 2017). Most of the relationships were evaluated at a long-term scale (Abatzoglou and Ficklin, 2017; Gentine et al., 2012; Li et al., 2013; Xu et al., 2013; Yang et al., 2009; Yang et al., 2007; Zhang et al., 2016c) due to the steady-state assumption of the Budyko model. However, hydrological processes, such as water storage, are usually nonstationary due to climate change and human activities (Greve et al., 2015; Ye et al., 2015). It should be noted here that the variability of controlling parameters from year to year may be considerably large in a specific river basin, which can be significantly affected by variations in vegetation cover and climate conditions. Hence, it is necessary to develop a model to estimate annual variations of controlling parameters. In a recent study, Ning et al. (2017) established an empirical relationship of the controlling parameter at the annual scale in the Loess Plateau of China. However, the annual values of the optimized controlling parameter in their study were calibrated with the *Fu* equation without consideration of the annual water storage changes (ΔS). But ΔS was identified as a key factor causing annual variations of water balance in most river basins, particularly in river basins of arid regions (e.g. Chen et al., 2013). Therefore, considering water storage changes, the effective precipitation (P_e), which is the difference between precipitation and water storage change (Chen et al., 2013), was used to extend the Budyko framework to annual-scale water balance analysis and was used to calibrate *n*.

Climate seasonality (SI) was identified to reflect the non-uniformity in the intra-annual distribution of water and energy, which plays a role in the variation of controlling parameter in the Budyko model (Woods, 2003; Ning et al., 2017; Yang et al., 2012). It is noted that distributions of water and energy were reflected not only by differences of seasonal amplitudes of P and E_0 but also by the phase mismatch between P and E_0. In this case, we proposed a climate seasonality and asynchrony index (SAI) to reflect the seasonality and asynchrony of water and energy distribution. Vegetation coverage has also been found to be closely related to the spatial variation of the controlling parameter (Yang et al., 2009). Li et al. (2013) and Xu et al. (2013) used vegetation coverage to model the spatial variation of the controlling parameter in 26 river basins over the globe at a long-term scale. However, the effect of climate variability was not considered, and the impact of vegetation dynamics on the temporal variation of the controlling parameter was not fully investigated. Zhang et al. (2016c) established the relationship of parameter *n* with vegetation changes over northern China and suggested that the relationship needed to be further assessed in other river basins across the globe. Also, they confirmed the impact of climate seasonality on parameter *n*, and suggested future studies on its impacts on *n*. Therefore, this study devepoed a semi-empirical formula for parameter *n* with SAI and M as predictor variables at the annual scale, using meteorological and hydrological data from 26 large river basins from around the globe with a broad range of climate conditions.

Much work has been done, addressing water balance variations (e.g., Liu et al., 2017a; Zeng and Cai, 2016; Zhang et al., 2016a; Zhang et al., 2016b). For instance, Zeng and Cai (2016) evaluated the impacts of P, E_0 and ΔS on the temporal variation of evaportranspiration for large river basins. However, little is known about the influence of M and SAI on the hydrological cycle, particularly on their contributions to variations of runoff and evapotranspiration. The impact of M and SAI on the water balance is critical for water balance modelling. Therefore, based on the developed semi-empirical formula, this study further assessed the causes of variation of R and E. Therefore, the objectives of this study were: (1) to propose a climate seasonality and asynchrony index, SAI, to reflect the mismatch of water and energy; (2) to develop an empirical model for the controlling parameter *n* at the annual scale using data from 26 large river basins from around the globe; and (3) to investigate the impact of SAI and other factors on the R and E variations.

2. Data

Monthly terrestrial water budget data covering a period of 1984-2006 was collected from 32 large river basins from around the globe (Pan et al., 2012). The data set, including P, E, R and ΔS, combined data from multiple sources, such as in situ observations, remote sensing retrievals, model simulations, and global reanalysis products, which was obtained using assimilation weighted with the estimated error. For more details on this dataset, reference can be made to Pan et al. (2012). This dataset, which was deemed to one of the best water budget estimates, has already been applied to assess the impact of vegetation, topography, latitude, and terrestrial storage on the spatial variability of the controlling parameter in the Budyko framework and the evapotranspiration variability over the past several years (Arnell and Gosling, 2013; Li et al., 2013; Xu et al., 2013; Zeng and Cai, 2016). The dataset has been designed to explicitly close the water budget. And that the use of data assimilation might lead to unphysical variability. As a result, Li et al. (2013) found that more than 20% of data in six basins among the 32 global basins were beyond the energy and water limits, and suggested analysis on water-energy balance using the remaining 26 basins. Following Li et al. (2013), we evaluated the impact of climate variability and vegetation dynamics on the spatiotemporal variation of the controlling parameter and the water balance of the 26 river basins. Detailed information about the characteristics of the 26 basins is given in Table 1. Monthly potential evapotranspiration (E_0) data from 1901 to 2015 at a spatial resolution of 0.5° was obtained from Climatic Research Unit of University of East Anglia (https://crudata.uea.ac.uk/cru/data/hrg/cru_ts_3.24.01/cruts.1701201703.v3.24.01/pet/). Monthly normalized difference vegetation index (NDVI) covering a period of 1981-2006 was obtained from Global Inventory Modeling and Mapping Studies (GIMMS) (Buermann, 2002; Li et al., 2013).

3. Methods

3.1 The Budyko framework at annual scale

Based on the Budyko framework, Choudhury (1999) and Yang et al. (2008) deduced a water-energy formula as:

$$E = \frac{PE_0}{(P^n + E_0^n)^{1/n}} \tag{1}$$

where n is the controlling parameter of the Choudhury-Yang equation which is one of the formulations of the Budyko framework.

The basin stores precipitation first and then releases it as runoff and evapotranspiration (Biswal, 2016). Affected by water storage changes, E is always not equal to the difference between P and R for a short time interval. Previous studies have found that storage changes have impacts on water balance at the annual scale (Donohue et al., 2012). To consider the influence of variation of water storage, Wang (2012) suggested to use effective precipitation (P_e), i.e., $P_e = P - \Delta S$, to replace precipitation in the water-energy balance. As a result, using the P_e, the Choudhury and Yang equation (1999) can be extended in short time scale:

$$R = P_e - \frac{P_e E_0}{({P_e}^n + E_0^n)^{1/n}} \tag{2a}$$

$$E = \frac{P_e E_0}{({P_e}^n + E_0^n)^{1/n}} \tag{2b}$$

Parameter n controls the shape of the Budyko curve and can be calibrated by minimizing the mean absolute error (*MAE*) (Legates and McCabe, 1999; Yang et al., 2007). Parameter n is a catchment characteristic parameter which is mainly related to the underlying conditions (i.e., topography and soil), climate conditions, and vegetation cover (Liu et al., 2017a; Yang et al., 2009; Zhang et al., 2016c). The underlying characteristics are relatively stable during a short time interval, while climate and vegetation might undergo considerable variations, which can lead to the change of parameter *n*. As a result, vegetation dynamics and climate variability were applied to simulate *n* and assess their impact on runoff and evapotranspiration.

The vegetation coverage (*M*), which is the fraction of land surface covered with green vegetation in the region, can be calculated as (Gutman and Ignatov, 1998):

$$M = (NDVI - NDVI_{min})/(NDVI_{max} - NDVI_{min}) \tag{3}$$

where $NDVI_{max}$ and $NDVI_{min}$ represent the dense green vegetation and bare soil with $NDVI_{max} = 0.80$ and $NDVI_{min} = 0.05$, respectively (Li et al., 2013; Ning et al., 2017; Yang et al., 2009).

3.2 Seasonality and asynchrony of water and energy

The seasonality of *P* and E_0, which are mainly controlled by solar radiation, follows a sine distribution (Milly, 1994; Woods, 2003):

$$P(t) = \bar{P}\left(1 + \delta_P \sin\left(\frac{2\pi}{\tau}\frac{t}{12}\right)\right) \tag{4a}$$

$$E_0(t) = \overline{E_0}\left(1 + \delta_{E_0} \sin\left(\frac{2\pi}{\tau}\frac{t}{12}\right)\right) \tag{4b}$$

where *t* is the time (months), *P*(*t*) and E_0 (*t*) are the monthly *P* and E_0 with the annual mean value of $\bar{P}$ and of $\overline{E_0}$, respectively. The quantities δ_P and δ_{E_0} are dimensionless seasonal amplitudes, which can be calibrated by minimizing *MAE*. The quantity τ is the cycle of seasonality, with half a year in the tropics and one year outside the tropics. The origin of time ($t = 0$) was fixed in April in the previous studies (Milly, 1994; Woods, 2003; Ning et al., 2017). As a result, if the δ_P (δ_{E_0}) was positive, the month with maximum monthly *P* (E_0) would appear in July, which corresponds to Northern Hemisphere (e.g., Figure 1a); while the southern Hemisphere would show a January maximum with negative δ_P (δ_{E_0}). Considering the difference between seasonal *P* and E_0, Wood et al. (2003) defined a climate seasonality index by combining Eq. (4):

$$\mathrm{SI} = |\delta_P - \delta_{E_0} DI| \tag{5}$$

where DI is the dryness index ($\frac{\overline{E_0}}{\overline{P}}$).

<Figure 1 here please>

Equations (4) - (5) were applied to represent the mismatch between water and energy (e.g., Ning et al., 2017). However, the following two issues still need to be considered: (1) effect of local climate and catchment characteristics, the phase of seasonal P and E_0 may be not entirely consistent with that of solar radiation; and (2) the phases between seasonal P and E_0 cannot always be consistent in a specific basin, such as the Northern Dvina basin (Figure 1b). The values of E for two basins with the same annual mean P, E_0, δ_P and δ_{E_0} can be different if the phases of seasonal P and E_0 are in mismatch. As a result, the phase shifts of P (S_P) and E_0 (S_{E_0}) should be considered in the sine function (Berghuijs and Woods, 2016):

$$P(t) = \overline{P}\left(1 + \delta_P \sin\left(\frac{2\pi}{\tau}\frac{t - S_P}{12}\right)\right) \tag{6a}$$

$$E_0(t) = \overline{E_0}\left(1 + \delta_{E_0} \sin\left(\frac{2\pi}{\tau}\frac{t - S_{E_0}}{12}\right)\right) \tag{6b}$$

As shown in figure 2, Eq. (6) with fitted phase performed much better in simulating monthly P and E_0 than eq. (4) with a fixed phase, with R^2 larger than 0.89 for the former but smaller than 0.64 for the latter.

<Figure 2 here please>

To fully reflect the difference between water and energy, it is necessary to consider not only the seasonal amplitude difference between P and E_0, but also the phase difference (i.e., asynchrony) between them (Fig S1b). Therefore, an improved climate index describing the difference between water and energy needs to be developed with the consideration of

Hydrol. Earth Syst. Sci. Discuss., https://doi.org/10.5194/hess-2018-200
Manuscript under review for journal Hydrol. Earth Syst. Sci.
Discussion started: 23 April 2018

seasonality and asynchrony of P and E_0. Based on eq. (6), we further deduced the following equations to express the difference between P and E_0:

$$\frac{P(t)-E_0(t)}{\bar{P}} = (1-DI) + \left(\delta_P \sin\left(\frac{2\pi}{\tau}\frac{t-S_P}{12}\right) - DI\,\delta_{E_0}\sin\left(\frac{2\pi}{\tau}\frac{t-S_{E_0}}{12}\right)\right)$$

$$= (1-DI) + (a^2+b^2)^{1/2}\sin\left(\frac{2\pi}{\tau}\frac{t}{12}-\varphi\right) \tag{7}$$

where $a = \delta_P\cos\delta_P - DI\delta_{E_0}\cos\frac{2\pi}{\tau}\frac{S_P}{12}$, $b = -\delta_P\sin\delta_P + DI\delta_{E_0}\sin\frac{2\pi}{\tau}\frac{S_{E_0}}{12}$, $\varphi = \arctan(b/a)$. Similar to *Milly* (1994), we defined a seasonality and asynchrony index (SAI) to reflect the mismatch between water and energy in terms of the magnitude and phase difference between P and E_0:

$$\mathrm{SAI} = (a^2+b^2)^{1/2}$$

$$= \left({\delta_P}^2 - 2\delta_P\delta_{E_0}DI\cos\left(\frac{2\pi}{\tau}\frac{S_P-S_{E_0}}{12}\right) + \left(\delta_{E_0}DI\right)^2\right)^{1/2} \tag{8}$$

The SI value calculated by eq. (5) was an exceptional case for P and E_0 in the same phase shifts. A larger SAI implies a greater difference between P and E_0 in the year. Besides, SAI followed the following three scenarios: (1) $\mathrm{SAI} < 1-\mathrm{DI}$, given a wet climate with $P(t) > E_0(t)$ across the whole seasonal cycle; (2) $\mathrm{SAI} < \mathrm{DI}-1$, given a dry climate with $P(t) < E_0(t)$ across the whole seasonal cycle; (3) $\mathrm{SAI} > |\mathrm{DI}-1|$, given that a larger SAI implies more surplus of P for the wet season with $P(t) > E_0(t)$.

3.3 Contributions of SAI and other factors to R and E

From eq. (2), we can redefine the total differential of R and E for any time scale by introducing effective precipitation (P_e):

$$\mathrm{d}R = \frac{\partial R}{\partial P_e}\mathrm{d}P_e + \frac{\partial R}{\partial E_0}\mathrm{d}E_0 + \frac{\partial R}{\partial n}\mathrm{d}n \tag{9a}$$

$$\mathrm{d}E = \frac{\partial E}{\partial P_e}\mathrm{d}P_e + \frac{\partial E}{\partial E_0}\mathrm{d}E_0 + \frac{\partial E}{\partial n}\mathrm{d}n \tag{9b}$$

The climatic elasticity of evapotranspiration changes to the changes of precipitation, potential evapotranspiration and *n* can be separately be expressed d as $\varepsilon_{P_e} = \frac{P_e}{E}\frac{\partial f}{\partial P_e}$, $\varepsilon_{E_0} = \frac{E_0}{E}\frac{\partial f}{\partial E_0}$, $\varepsilon_n = \frac{n}{E}\frac{\partial f}{\partial n}$. The climatic elasticity of runoff changes is similar to the climatic elasticity evapotranspiration changes. The difference operator (d) in eq. (9a) and eq. (9b) refer to the difference of a variable before and after change points of *R* and *E*, respectively. The relative contribution (C) of P_e, E_0 and n to the *R* and *E* changes can be obtained as:

$$C_{P_e} = \frac{|I_{P_e}|}{|I_P| + |I_{E_0}| + |I_n|},\ C_{E_0} = \frac{|I_{E_0}|}{|I_P| + |I_{E_0}| + |I_n|},\ C_n = \frac{|I_n|}{|I_P| + |I_{E_0}| + |I_n|} \quad (10)$$

I_{P_e}, I_{E_0} and I_n denote, respectively, the impacts of P_e, E_0 and n on *R* or *E*, which can be expressed by $\frac{\partial E}{\partial P_e}\mathrm{d}P_e, \frac{\partial E}{\partial E_0}\mathrm{d}E_0$ and $\frac{\partial E}{\partial n}\mathrm{d}n$, respectively. After getting the contribution of *n* to the *R* and *E* variations, we can further assess the impacts of M and SAI on the variation of *R* and *E*, based on the semi-empirical model of *n* in terms of M and SAI. Following Ning et al. (2017), the changes of parameter *n* can be expressed as follows:

$$\mathrm{d}n = \frac{\partial n}{\partial \mathrm{SAI}}\mathrm{dSAI} + \frac{\partial n}{\partial \mathrm{M}}\mathrm{dM} \quad (11)$$

Then, the relative contributions of SAI (*C*_SAI) and M (*C*_M) to the changes of parameter *n* can be obtained. Combining with the contribution of *n* to the *R* and *E* changes, the relative contributions of SAI and M to the variations of *R* and *E* can be obtained:

$$C_{\mathrm{SAI}} = C_n \times \mathrm{C\_SAI},\ \ C_{\mathrm{M}} = C_{\mathrm{n}} \times C\_\mathrm{M} \quad (12)$$

4. Results

4.1 Performance of the proposed SAI in the Budyko framework

Figure 2 shows that eq. (6) with SAI has a better performance in simulating *P* and E_0 than eq. (4) with SI. Here we further assessed the performance of these two indices, by comparing with the controlling parameter *n* in the Budyko framework. Parameter *n* for each year was first

Hydrol. Earth Syst. Sci. Discuss., https://doi.org/10.5194/hess-2018-200
Manuscript under review for journal Hydrol. Earth Syst. Sci.
Discussion started: 23 April 2018

calibrated by eq. (2). The calibrated parameter n was called optimized n. For the representativeness of the relation between n and other factors, analysis was done at a larger spatial scale with different climate conditions by combining data from 26 global large basins (Figure 3). The correlation coefficient (r) between SI and optimized n was 0.47 (Figure 3a). If the asynchrony of seasonal P and E_0 was considered in SI, i.e., SAI, r increased to 0.68 (Figure 3b). In addition, the accuracy of simulated n using SAI as a predictor was higher than that using SI, i.e., R^2 was 0.46 for the former compared to 0.22 for the latter (Figure 4a and 4b). In short, although SI showed a significant relationship with n, SAI considering both seasonality and asynchrony of P and E_0 was more applicable to represent the difference between water and energy, and better performed in the simulation of n in the Budyko model.

<Figure 4 here please>

To further assess the impact of SAI on the fluvial water balance, we also analyzed the roles of SAI in Budyko framework and climate elasticity (Figure 3e, Figure 5). As shown in Figure 3e, a larger value of n was related to a higher evapotranspiration ratio for a given aridity index, and as SAI increased, the value of controlling parameter n tended to decrease. In other words, catchments with a larger SAI had a lower evapotranspiration ratio given the same aridity index. This result is similar to the finding from Zhang et al (2015), who found that a larger snow ratio caused a higher runoff index for a given dryness index. In contrast, this relationship is not distinct for SI (Figure 3d).

Figure 5 shows the spatial patterns of climate elasticities and their relationship with SAI. The climate elasticities of precipitation and parameter n to evapotranspiration increased with SAI, whereas the elasticity of potential evapotranspiration to evapotranspiration decreased with SAI

(Figure 5), implying that the variation of evapotranspiration in the catchments with a higher SAI were more sensitive to the changes of precipitation and parameter *n*, but less sensitive to the changes of potential evapotranspiration.

<Figure 5 here please>

4.2 A semi-empirical formula for parameter n

Previous studies have found that vegetation cover is closely related to the spatial variation of *n* in different regions (e.g., Li et al. 2013). However, the new finding in this study is that vegetation dynamics (M) also has a significant impact on the temporal variation of annual values of parameter *n* (Figure 3c; Figure 4c) and evapotranspiration ratio (Figure 3f). As shown in Figure 4c, M can explain 67% of spatiotemporal variance of annual *n* with *MAE* of 0.28. Nevertheless, the simulation accuracy of *n* can be further improved, particularly at the high end. As mentioned above, SAI has a significant impact on the variation of *n*. Therefore, based on the results obtained by Li et al. (2013), it is possible to develop a more dynamic model to capture the spatiotemporal variation of parameter *n*, and improve the simulation of *n* by incorporating SAI into the empirical model.

Following the phenomenological considerations and the relationships demonstrated in Figures 3b and 3c, the limiting conditions of SAI and M were achieved: (1) If SAI $\rightarrow +\infty$, which indicates that the match of P and E_0 tends to be the worst, and thus $R \rightarrow P$ and $E \rightarrow 0$, i.e., $n \rightarrow 0$; (2) When $\mathrm{M} \uparrow$, then $E \uparrow$, which has been demonstrated by previous studies (i.e., Yang et al., 2009; Li et al., 2013), and thus $n \uparrow$, which can also be found in Figures 3c and 3f. Based on these limiting conditions, a semi-empirical formula for parameter *n* was obtained as:

$$n = a\mathrm{SAI}^b\mathrm{M}^c \tag{13}$$

Hydrol. Earth Syst. Sci. Discuss., https://doi.org/10.5194/hess-2018-200
Manuscript under review for journal Hydrol. Earth Syst. Sci.
Discussion started: 23 April 2018

where *a* and *b* are positive regression coefficients and c is negative. Nonlinear least squares can be used to estimate the values of *a*, *b*, and *c*, based on *n* calibrated from measured data. Then, the final equation was as follows

$$n = 0.27\mathrm{SAI}^{-0.30}\mathrm{M}^{0.90} \tag{14}$$

As shown in Figure 4d, the simulated *n* calculated by semi-empirical formula match well with the optimized *n* with R^2 of 0.82 and *MAE* of 0.2.

In addition to the semi-empirical formulae, multiple linear regression (MLR) is often applied to simulate *n*. For example, taking NDVI, latitude, and topographic index as explanatory variables, Xu et al. (2013) applied MLR to estimate the spatial variation of *n* for the global large river basins. Accordingly, we also fitted parameter *n* by MLR. As shown in Figure 4e, the values of R^2 and MAE of the simulated *n* by using MLR were 0.72 and 0.23, respectively, which was not as good as the performance of the semi-empirical formulae. Therefore, the semi-empirical formula was a better choice not only for simulation but also for explaining the physical meaning.

Cross-validation was used to validate the semi-empirical equation. The dataset for one basin was used for validation, and the dataset for the remaining 25 basins were used for calibration. Then the cross-validation process is repeated 26 times, with each of 26 basins used once as validation. Parameter *n* for the validation basin was simulated by the semi-empirical formula obtained from the other 25 basins. Subsequently, based on annual P_e, E_0 and simulated annual parameter *n*, simulated annual *R* and *E* were calculated using eq. (2). The simulated annual *R* and *E* for each validation basin were combined to compare with the observed *R* and *E*, respectively. As shown in Figure 6, the simulated annual *R* and *E* showed a remarkable agreement with the observed ones with R^2 larger than 0.96 and MAE smaller than 35 mm. These results indicated that the semi-empirical formula expressed the spatiotemporal variation of parameter *n*, and the proposed eq. (2) with simulated parameter *n* was reliable for the simulation of annual *R* and *E*.

<Figure 6 here please>

4.3 Contributions of SAI and other factors to R and E changes

To further assess the impact of SAI on the water balance, here we quantified the contributions of SAI and other factors, i.e. P_e, E_0 and M, on the variation of *R* and *E* (Figures 7 and 8). As can be seen from Figures 7a and 7c, the P_e changes controlled the variation of *R* in most basins, with 18 of the 26 selected basins. The contributions of P_e changes to *R* changes ranged from 11% to 96% with the median value at 61% for the 26 basins (Fig 7b). In addition to the P_e changes, the SAI change was also an important factor for the *R* change with the median contribution at 15%. SAI was the dominant factor with the maximum contribution to *R* changes in six rivers, such as Yangtze, Yellow, Aral, Northern Dvina, Congo and Mississippi basin. The E_0 changes had a limited impact on the *R* changes with the median contribution of 8%. However, it is the dominant factor for *R* changes in Danube River basins.

<Figures 7 and 8 here please>

The dominant factors of *E* changes were different from those of *R* changes (Figure 8). Both the SAI and M changes had remarkable impacts on the *E* changes, which were the dominant factors for the *E* changes within eight and five basins, respectively. Also, the contributions of SAI and M changes to *E* changes were larger than those to *R* changes with the median contributions of 19% and 21%, respectively. Accordingly, the contribution of P_e to *E* changes was weaker than that to *R* changes, the median of which dropped from 61% to 35%.

In summary, P_e was the key controlling factor for *R* and *E* in most river basins. SAI was the dominant factor for both *R* and *E* mainly in East Asian subtropical monsoon zones, such as Yangtze and Yellow River basins. M was the dominant factor for both *R* and *E* in the temperate grassland zone of South America, i.e., Parana River basin. E_0 had a limited impact on both *R* and *E*, but it is the dominant factor for both *R* and *E* changes in temperate maritime climate of Europe, i.e., Danube River basin.

5. Discussion

It has been found that both vegetation coverage and climate seasonality have impacts on water balance (Chen et al., 2013; Li et al., 2013; Zeng and Cai, 2016; Abatzoglou and Ficklin, 2017; Ning et al., 2017; Zhang et al., 2016a). Li et al. (2013) found that long-term vegetation coverage was closely related to the spatial variation of the calibrated parameter of the Budyko model in global river basins. However, vegetation dynamics also influenced the temporal variation of parameter *n*, but the relationship remained to be verified over a larger spatial range (Zhang et al., 2016c; Ning et al., 2017). Results of this study confirmed that the vegetation dynamics had a significant impact on both spatial and temporal variations of the controlling parameter *n* at the global scale.

The seasonality index represents the amplitude difference of seasonal *P* and E_0, but does not include the phase difference of seasonal *P* and E_0. Investigating the water balance across the Loess Plateau in China, Ning et al. (2017) found that seasonal index, SI, was closely related to the controlling parameter. In this study, however, SI showed a worse correlation with the variation of *n* in the 26 large global river basins than those in Loess Plateau. All catchments

Hydrol. Earth Syst. Sci. Discuss., https://doi.org/10.5194/hess-2018-200
Manuscript under review for journal Hydrol. Earth Syst. Sci.
Discussion started: 23 April 2018

selected by Ning et al. (2017) were in the monsoon climate zone, where water and energy are strongly coupled, so the seasonality of P and E_0 in most catchments was in the same phase. Hence, the asynchrony of water and energy was nonexistent and had a limited impact on the variation of n. In contrast, the basins selected in this study covered a large spatial scale with a wide range of climate types. Most basins had different phases between seasonal P and E_0, such as the Northern Dvina with the phase differences larger than two months. The amplitude difference between seasonal P and E_0 cannot adequately represent the difference between water and energy in the basins with out-of-phase P and E_0 (Hickel and Zhang, 2006). In this case, SAI, considering both amplitude and phase differences between seasonal of P and E_0, was proposed to reflect the difference between water and energy. Results showed that the proposed SAI had a significant impact on n and evapotranspiration radio, as well as the sensitively of evapotranspiration to the variation of precipitation, potential evapotranspiration, and catchments characteristics. SAI can also be applied to other studies on water-energy balance.

In small-size catchments, interactions between climate variability, vegetation dynamics, and water balance are more complex (Li et al., 2013). Many other factors, such as basins area, latitude, slope gradient, compound topographic index, and so on (Abatzoglou and Ficklin, 2017; Xu et al., 2013; Yang et al., 2009), have been identified to play a role in the spatial distribution of n for small-size catchments. However, in this study, these factors had little changes at the annual time scale, so they were not considered in determining the annual variation of n. This study demonstrated that SAI and M play an important role in the spatiotemporal variation of n in large river basins, nevertheless, other factors should also be considered in the simulation of spatial variation of n for small-size catchments.

SAI was identified to have a great influence on the changes of R and E. Especially, the changes of both R and E for the two major rivers (i.e., Yangtze and Yellow River basins) in East Asian monsoon zone is mainly controlled by SAI. Hoyos and Webster, (2007) found that the variation of monsoon systems remarkably affects the climate seasonal pattern (Hoyos and Webster, 2007). Using the covariance of P and E_0 as an explanatory variable, Zeng and Cai (2016) indicated that the seasonality of P and E_0 had a significant impact on the E variation, such as the Yangtze River basin. Their results are generally consistent with ours. To assess the impact of ecological restoration on runoff in the Loess Plateau of China, Liang et al. (2015) regarded the ecological restoration, i.e., vegetation dynamics, as the cause of changes in n. However, our results showed that SAI also played an important role in the changes of n, particularly for the East Asian subtropical monsoon zone.

E_0 is the mainly controlling factor for the changes of both R and E in Danube river. The increased air temperature (Busuioc et al, 2010) increase the potential evapotranspiration significantly for the Danube river, which make a deficit increase and a decrease of excess water from precipitation (Bandoc et al., 2012). As a result, the R and E in Danube river was significantly affected by the E_0.

Although SAI combined with M can well capture the changes of n (Figure 4d), the impact of n on the water balance not only includes SAI and M, but also the human influence, which has been verified by our previous study (Liu et al., 2017a). As a result, this may cause uncertainty in our findings. The human influences on R and E need to be further investigated.

6. Conclusions

In this study, a semi-empirical formula was developed to simulate the spatiotemporal variation of the controlling parameter *n* in the Budyko model. Influences of climate-vegetation factors on water balance were evaluated. The Choudhury-Yang equation modified by the effective precipitation is recommended to calibrate the controlling parameter *n* and to simulate evapotranspiration (*E*) and runoff (*R*), and their variation.

A climate seasonality and asynchrony index, i.e., SAI, is proposed to reflect the difference between water and energy. Results show that the optimized *n* has a much higher correlation with SAI than the existing SI, implying that the phase mismatch between seasonal water and energy should be considered in the impact assessment of water balance. In general, our results suggest that the catchments with a larger SAI usually have a larger evapotranspiration ratio given the same climatic and underlying condition, and the variation of evapotranspiration tends to be more sensitive to the changes of precipitation and landscape properties (parameter *n*), whereas less sensitive to the potential evapotranspiration in the catchments with larger SAI. Furthermore, this study confirms that vegetation dynamics (M) also plays an important role in modifying the temporal variation of *n* at the annual scale. Based on SAI and M, a semi-empirical formula for the spatiotemporal variation of parameter *n* has been developed, and it performs well in the prediction of annual evapotranspiration and runoff.

Employing the developed semi-empirical formula, the contributions of SAI and M, as well as P_e and E_0, to the variation of *E* and *R* were assessed. Results show that precipitation is the first-order control on the *R* and *E* changes, and, secondly, SAI was found to control the changes of *R* and *E* in the subtropical monsoon regions of East Asian. SAI, M and E_0 have large impacts on E than on R, whereas P_e has larger impacts on R.

The study assesses the influence of climate variability and vegetation dynamics on water balance, which highlights the role of climate seasonality and asynchrony as well as vegetation dynamics in the annual variation of n, and sheds new light on the difference in the contributions of climate-vegetation factors to the changes in R and E. This study can be useful for water-energy modelling, hydrological forecasting, and water management.

Acknowledgments: This work is financially supported by the National Science Foundation for Distinguished Young Scholars of China (Grant No.: 51425903), the Fund for Creative Research Groups of National Natural Science Foundation of China (Grant No.: 41621061), National Natural Science Foundation of China (No. 41771536) and by Key Project of National Natural Science Foundation of China (Grant No.: 51190091), National Natural Science Foundation of China under Grant No. 41401052. We would like to thank Ming Pan (mpan@princeton.edu), Dan Li (danl@princeton.edu) at Princeton University and Xianli Xu (xuxianliww@gmail.com) at Chinese Academy of Sciences for sharing basin data set. Information of the data were provided with great details in the Data section and further message concerning data please write to zhangq68@bnu.edu.cn.

References

Abatzoglou, J. T., and Ficklin, D. L.: Climatic and physiographic controls of spatial variability in surface water balance over the contiguous United States using the Budyko relationship, Water Resour. Res., 10.1002/2017wr020843, 2017.

Hydrol. Earth Syst. Sci. Discuss., https://doi.org/10.5194/hess-2018-200
Manuscript under review for journal Hydrol. Earth Syst. Sci.
Discussion started: 23 April 2018

Hydrology and Earth System Sciences
Open Access
Discussions

Arnell, N. W., and Gosling, S. N.: The impacts of climate change on river flow regimes at the global scale, J. Hydrol., 486, 351-364, 2013.

Bandoc, G.: Estimation of the annual and interannual variation of potential evapotranspiration, Evapotranspiration-Remote Sensing and Modeling, InTech, 251-272, 2012.

Berghuijs, W. R., & Woods, R. A.: A simple framework to quantitatively describe monthly precipitation and temperature climatology, Int. J. Climatology, 36(9), 3161-3174, 2016.

Biswal, B.: Dynamic hydrologic modeling using the zero-parameter Budyko model with instantaneous dryness index, Geophys. Res. Lett., 43, 9696-9703, 10.1002/2016gl070173, 2016.

Buermann, W.: Analysis of a multiyear global vegetation leaf area index data set, J. Geophys. Res.-Atmos., 107, 10.1029/2001jd000975, 2002.

Busuioc,A; Caian, M.; Cheval, S.; Bojariu, R.; Boroneant, C.; Baciu, M.; Dumitrescu, A.: Climate variability and change in Romania, Ed. ProUniversitaria, 59-72, ISBN 978-973-129-549-7, Bucureşti, România 2010.

Cai, D., Fraedrich, K., Sielmann, F., Guan, Y., Guo, S., Zhang, L., and Zhu, X.: Climate and vegetation: An ERA-interim and GIMMS NDVI analysis, J. Climate, 27, 5111-5118, 2014.

Chen, X., Alimohammadi, N., and Wang, D.: Modeling interannual variability of seasonal evaporation and storage change based on the extended Budyko framework, Water Resour. Res., 49, 6067-6078, 10.1002/wrcr.20493, 2013.

Choudhury, B.: Evaluation of an empirical equation for annual evaporation using field observations and results from a biophysical model, J. Hydrol., 216, 99-110, 1999.

Dagon, K., and Schrag, D. P.: Exploring the effects of solar radiation management on water cycling in a coupled land–atmosphere model. J. Climate, 29, 2635-2650, 2016.

Donohue, R. J., Roderick, M. L., and McVicar, T. R.: Roots, storms and soil pores: Incorporating key ecohydrological processes into Budyko's hydrological model, J. Hydrol., 436-437, 35-50, 10.1016/j.jhydrol.2012.02.033, 2012.

Fu, B. P.: On the calculation of the evaporation from land surface, Sci. Atmos. Sin., 5, 23-31, 1981 (in Chinese).

Gentine, P., D'Odorico, P., Lintner, B. R., Sivandran, G., and Salvucci, G.: Interdependence of climate, soil, and vegetation as constrained by the Budyko curve, Geophys. Res. Lett., 39, n/a-n/a, 10.1029/2012gl053492, 2012.

Greve, P., Gudmundsson, L., Orlowsky, B., and S. I. Seneviratne: The Budyko framework beyond stationarity, Hydrol. Earth Syst. Sci. Discuss, 12, 6799–6830, 2015.

Gutman, G., and Ignatov, A.: The derivation of the green vegetation fraction from NOAA/AVHRR data for use in numerical weather prediction models, Int. J. Remote Sens., 19, 1533-1543, 1998.

Hickel, K., and Zhang, L.: Estimating the impact of rainfall seasonality on mean annual water balance using a top-down approach, J. Hydrol., 331, 409–424, 2006.

Hoyos, C. D., and Webster, P. J.: The role of intraseasonal variability in the nature of Asian monsoon precipitation, J. Climate, 17, 4402-4424, 2007.

Koster, R. D. and Suarez, M. J.: A simple framework for examining the interannual variability of land surface moisture fluxes, J. Climate, 12, 1911-1917, 1999.

Legates, D. R., and McCabe, G. J.: Evaluating the use of "goodness - of - fit" measures in hydrologic and hydroclimatic model validation, Water Resour. Res., 35, 233-241, 1999.

Li, D., Pan, M., Cong, Z., Zhang, L., and Wood, E.: Vegetation control on water and energy balance within the Budyko framework, Water Resour. Res., 49, 969-976, 10.1002/wrcr.20107, 2013.

Liang, W., Bai, D., Wang, F., Fu, B., Yan, J., Wang, S., Yang, Y., Long, D., and Feng, M.: Quantifying the impacts of climate change and ecological restoration on streamflow changes based on a Budyko hydrological model in China's Loess Plateau, Water Resour. Res., 51, 6500-6519, 2015.

Liu, J., Zhang, Q., Singh, V. P., and Shi, P.: Contribution of multiple climatic variables and human activities to streamflow changes across China, J. Hydrol., 545, 145-162, 2017a.

Liu, J., Zhang, Q., Zhang, Y., Chen, X., Li, J., and Aryal, S. K.: Deducing climatic elasticity to assess projected climate change impacts on streamflow change across China, J. Geophys. Res.-Atmos., 2017b.

Milly, P. C. D.: Climate, soil water storage, and the average annual water balance, Water Resour. Res., 30, 2143-2156, 1994.

Ning, T., Li, Z., and Liu, W.: Vegetation dynamics and climate seasonality jointly control the interannual catchment water balance in the Loess Plateau under the Budyko framework, Hydrol. Earth Syst. Sci., 21, 1515-1526, 10.5194/hess-21-1515-2017, 2017.

Pan, M., Sahoo, A. K., Troy, T. J., Vinukollu, R. K., Sheffield, J., and Wood, E. F.: Multisource Estimation of Long-Term Terrestrial Water Budget for Major Global River Basins, J. Climate, 25, 3191-3206, 10.1175/jcli-d-11-00300.1, 2012.

Potter, N. J., Zhang, L., Milly, P. C. D., McMahon, T. A., and Jakeman, A. J.: Effects of rainfall seasonality and soil moisture capacity on mean annual water balance for Australian catchments, Water Resour. Res., 41, 10.1029/2004wr003697, 2005.

Wang, D., and Alimohammadi, N.: Responses of annual runoff, evaporation, and storage change to climate variability at the watershed scale, Water Resour. Res., 48, doi:10.1029/2011WR011444, 2012.

Weiss, M., and Coauthors: Contribution of dynamic vegetation phenology to decadal climate predictability, J. Climate, 27, 8563-8577, 2014.

Woods, R.: The relative roles of climate, soil, vegetation and topography in determining seasonal and long-term catchment dynamics, Adv. Water Resour., 26, 295-309, 2003.

Woods, R. A.: Analytical model of seasonal climate impacts on snow hydrology: Continuous snowpacks. Adv. Water Resour., 32, 1465-1481, doi:10.1016/j.advwatres.2009.06.011, 2009.

Xu, X., Liu, W., Scanlon, B. R., Zhang, L., and Pan, M.: Local and global factors controlling water-energy balances within the Budyko framework, Geophys. Res. Lett., 40, 6123-6129, 10.1002/2013gl058324, 2013.

Yan, J. W. and Coauthors: Changes in the land surface energy budget in eastern China over the past three decades: Contributions of land-cover change and climate change. J. Climate, 27, 9233-9252, 2014.

Yang, D., Sun, F., Liu, Z., Cong, Z., Ni, G., and Lei, Z.: Analyzing spatial and temporal variability of annual water-energy balance in nonhumid regions of China using the Budyko hypothesis, Water Resour. Res., 43, , 10.1029/2006wr005224, 2007.

Yang, D., Shao, W., Yeh, P. J. F., Yang, H., Kanae, S., and Oki, T.: Impact of vegetation coverage on regional water balance in the nonhumid regions of China, Water Resour. Res., 45, 10.1029/2008wr006948, 2009.

Yang, H., Yang, D., Lei, Z., and Sun, F.: New analytical derivation of the mean annual water-energy balance equation, Water Resour. Res., 44, n/a-n/a, 10.1029/2007wr006135, 2008.

Yang, H., Lv, H., Yang, D., and Hu, Q.: Seasonality of precipitation and potential evaporationanditsimpact on catchment waterenergy balance , Journal of Hydroelectric Engineering, Journal of Hydroelectric Engineering, 31, 54-59, 2012 (in Chinese).

Ye, S., Li, H.-Y., Li, S., Leung, L. R., Demissie, Y., Ran, Q., and Blöschl, a. G.: Vegetation regulation on streamflow intra‐annual variability through adaption to climate variations, Geophys. Res. Lett., 42, 10.1002/, 2015.

Zeng, R., and Cai, X.: Climatic and terrestrial storage control on evapotranspiration temporal variability: Analysis of river basins around the world, Geophys. Res. Lett., 43, 185-195, 10.1002/2015gl066470, 2016.

Zhang, D., Cong, Z., Ni, G., Yang, D., and Hu, S.: Effects of snow ratio on annual runoff within the Budyko framework. Hydrol. Earth Syst. Sci., 19, 1977-1992, 2015.

Zhang, D., Liu, X., Zhang, Q., Liang, K., and Liu, C.: Investigation of factors affecting intra-annual variability of evapotranspiration and streamflow under different climate conditions, J. Hydrol., 543, 759-769, 10.1016/j.jhydrol.2016.10.047, 2016a.

Zhang, Q., Liu, J., Singh, V. P., Gu, X., and Chen, X.: Evaluation of impacts of climate change and human activities on streamflow in the Poyang Lake basin, China, Hydrol. Process., 30, 2562-2576, 10.1002/hyp.10814, 2016b.

Zhang, S., Yang, H., Yang, D., and Jayawardena, A. W.: Quantifying the effect of vegetation change on the regional water balance within the Budyko framework, Geophys. Res. Lett., 43, 1140-1148, 10.1002/, 2016c.

562 Table 1. Long-term annual mean meteorological and hydrological characteristics and vegetation coverage

563 (1984-2006) for the 26 large river basins around the world.

Number	Basins	P (mm)	E_0 (mm)	ΔS (mm)	E (mm)	R (mm)	M	SAI	n
1	Amazon	2173	1284	6	1145	1022	9.2	0.5	2.3
2	Amur	411	756	-5	282	134	3.8	0.9	1.1
3	Aral	255	1129	-22	209	68	2.4	0.8	0.9
4	Columbia	566	916	-20	318	268	4.7	1.9	0.9
5	Congo	1371	1175	9	1008	354	8.8	0.2	3.3
6	Danube	733	742	-14	498	249	6.7	0.7	1.8
7	Indigirka	223	345	6	73	144	2.4	1.6	0.5
8	Indus	450	1315	-6	293	163	2.5	1.3	0.8
9	Kolyma	267	355	6	125	137	2.6	1.2	0.8
10	Lena	352	436	4	180	168	3.6	1.0	0.9
11	Mackenzie	392	462	2	212	178	4.4	1.0	1.0
12	Mississippi	776	1104	-3	578	201	6.1	0.7	1.6
13	Niger	616	1958	-10	423	202	3.2	1.5	0.8
14	Nile	543	1863	-2	421	124	3.7	0.7	1.0
15	Northern Dvina	588	479	-10	267	330	6.3	0.9	1.0
16	Ob	474	597	-2	275	200	4.7	1.1	1.1
17	Olenek	277	370	-2	113	166	2.5	1.4	0.7
18	Parana	1242	1307	-14	982	274	8.4	0.5	2.6
19	Pearl	1424	967	-7	627	804	6.1	0.7	1.2
20	Pechora	544	394	2	186	356	3.8	0.8	0.8
21	Senegal	318	2014	-8	284	41	2.0	2.2	1.0
22	Volga	568	651	-11	354	225	5.6	1.2	1.3
23	Yangtze	1000	857	-3	378	625	5.4	0.5	0.8
24	Yellow	424	919	-5	324	105	3.4	0.8	1.2
25	Yenisei	430	468	-6	227	209	4.3	0.8	1.0
26	Yukon	268	383	16	86	166	3.7	1.1	0.5

564

Hydrol. Earth Syst. Sci. Discuss., https://doi.org/10.5194/hess-2018-200
Manuscript under review for journal Hydrol. Earth Syst. Sci.
Discussion started: 23 April 2018

Figure captions

Figure 1. Two examples showing the mismatch between precipitation (*P*) and potential evapotranspiration (E_0), in terms of (a) seasonal amplitudes (δ_P, δ_{E_0}) and (b) phase shift (S_P, S_{E_0}).

Figure 2. Comparing the observed and simulated monthly precipitation and potential evapotranspiration, using the sine function with fixed phase (i.e., Eq. (4)) and fitted phase (i.e., Eq. (6)).

Figure 3. Relationship between optimized n and (a) SI, (b) SAI and (c) M. (d-f) Distribution of evapotranspiration ratio (E/P_e) as a function of the aridity index (E_0/P_e) classified by 26 global large river basins at annual scale. The Budyko curves from the top down are derived from eq. (2b) with n=∞, n=5, n=2, n=1, n=0.6 and n=0.4, respectively. Noted that each point represents one year based on the combined dataset from 26 global large basins.

Figure 4. Optimized (calibrated) *n* versus simulated *n* modeled by (a) SI, (b) SAI, (c) M, (d) M and SAI using the semi-empirical formula (SEF, eq. (14)), and (e) M and SAI using the multiple linear regression (MLR). Noted that each point represents one year based on the combined dataset from 26 global large basins.

Figure 5. The climatic elasticity of evapotranspiration to the changing precipitation, potential evaporation and other factors represented by controlling parameter *n* in the 26 global large river basins, and its relations with the climate seasonality and asynchrony index (SAI). Noted that each point represents one of the 26 global large basins.

Figure 6. Simulation versus observation for (a) annual evapotranspiration and (b) annual runoff by using Eq. (2) with the simulated parameter *n* regarding M and SAI as predictor using

Hydrol. Earth Syst. Sci. Discuss., https://doi.org/10.5194/hess-2018-200
Manuscript under review for journal Hydrol. Earth Syst. Sci.
Discussion started: 23 April 2018

the semi-empirical formula (i.e., eq. (14).

Figure 7. Relative contributions to the long-term mean changes of Runoff (before and after changepoint) from P_e, SAI, M) and E_0 changes. The distribution ranges of relative contribution for each factor are shown in (b) and the number of basins dominated by each factor with the largest relative contribution is summarized in (c).

Figure 8. The same as Figure 7 but for relative contribution to the changes of evapotranspiration.

Hydrol. Earth Syst. Sci. Discuss., https://doi.org/10.5194/hess-2018-200
Manuscript under review for journal Hydrol. Earth Syst. Sci.
Discussion started: 23 April 2018

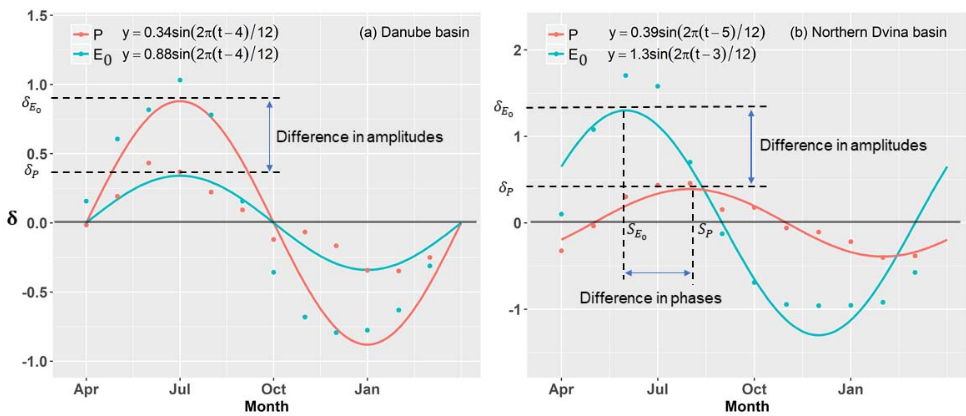

Figure 1. Two examples showing the mismatch between long-term monthly precipitation (P) and potential evapotranspiration (E_0), in terms of (a) seasonal amplitudes (δ_P, δ_{E_0}) and (b) phase shift (S_P, S_{E_0}).

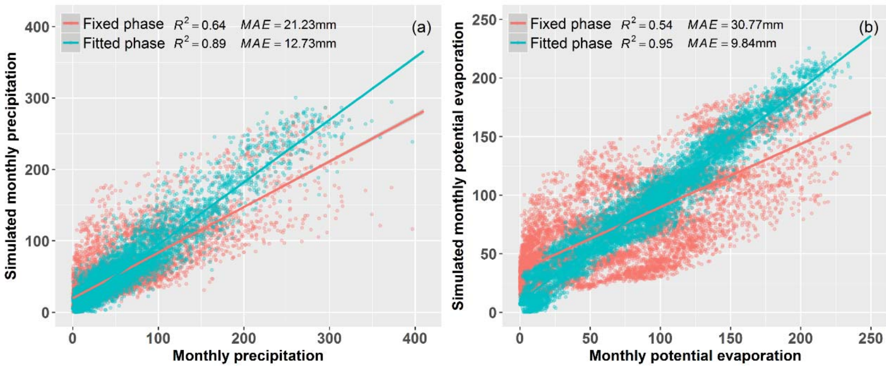

Figure 2. Comparing the observed and simulated monthly precipitation and potential evapotranspiration, using the sine function with fixed phase (i.e., Eq. (4)) and fitted phase (i.e., Eq. (6)). Noted that each point represents one-month data based on the combined dataset from 26 global large basins.

Hydrol. Earth Syst. Sci. Discuss., https://doi.org/10.5194/hess-2018-200
Manuscript under review for journal Hydrol. Earth Syst. Sci.
Discussion started: 23 April 2018

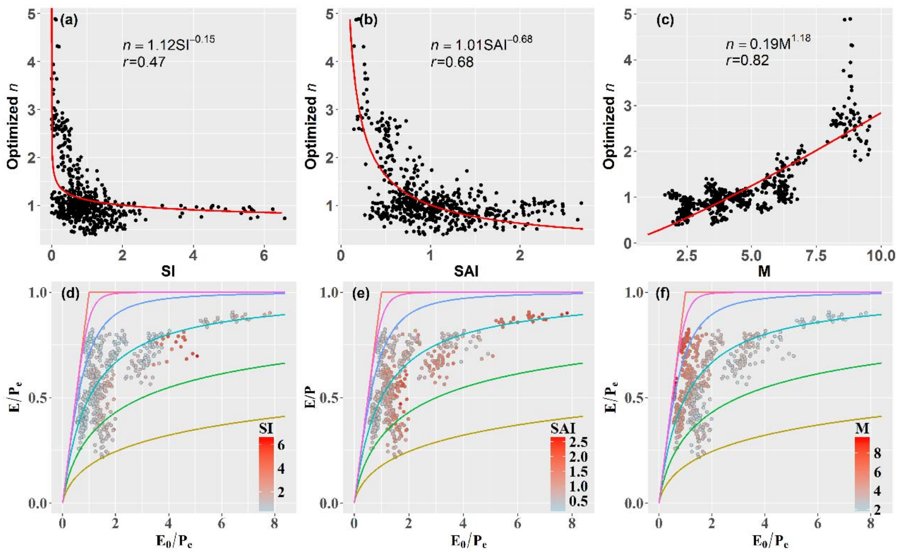

Figure 3. Relationship between optimized n and (a) SI, (b) SAI and (c) M. (d-f) Distribution of evapotranspiration ratio (E/P_e) as a function of the aridity index (E_0/P_e) classified by 26 global large river basins at annual scale. The Budyko curves from the top down are derived from eq. (2b) with n=∞, n=5, n=2, n=1, n=0.6 and n=0.4, respectively. Noted that each point represents one year based on the combined dataset from 26 global large basins.

Hydrol. Earth Syst. Sci. Discuss., https://doi.org/10.5194/hess-2018-200
Manuscript under review for journal Hydrol. Earth Syst. Sci.
Discussion started: 23 April 2018

Hydrology and Earth System Sciences
Open Access
Discussions

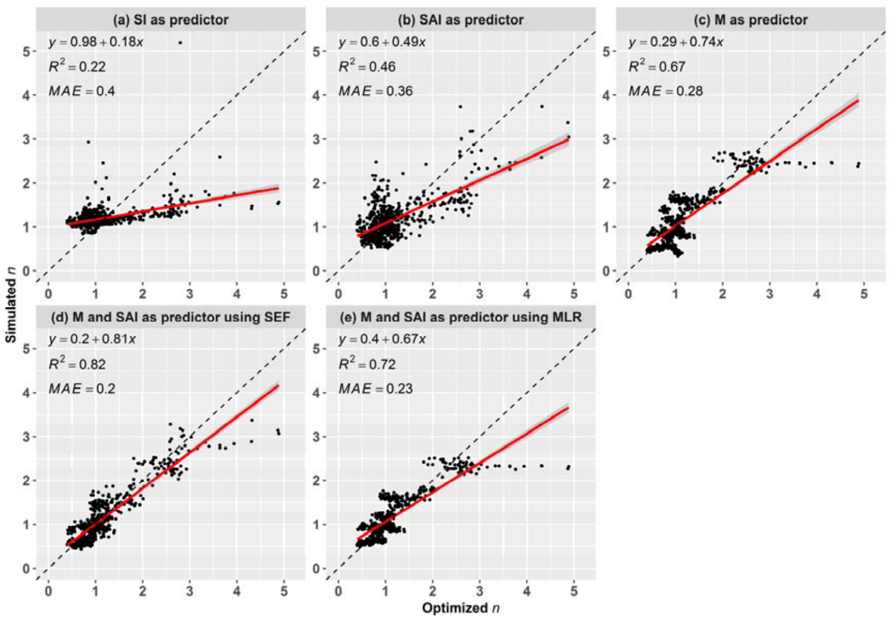

Figure 4. Optimized (calibrated) *n* versus simulated *n* modeled by (a) SI, (b) SAI, (c) M, (d) M and SAI using the semi-empirical formula (SEF, eq. (14)), and (e) M and SAI using the multiple linear regression (MLR). Noted that each point represents one year based on the combined dataset from 26 global large basins.

Hydrol. Earth Syst. Sci. Discuss., https://doi.org/10.5194/hess-2018-200
Manuscript under review for journal Hydrol. Earth Syst. Sci.
Discussion started: 23 April 2018

Hydrology and Earth System Sciences
Discussions

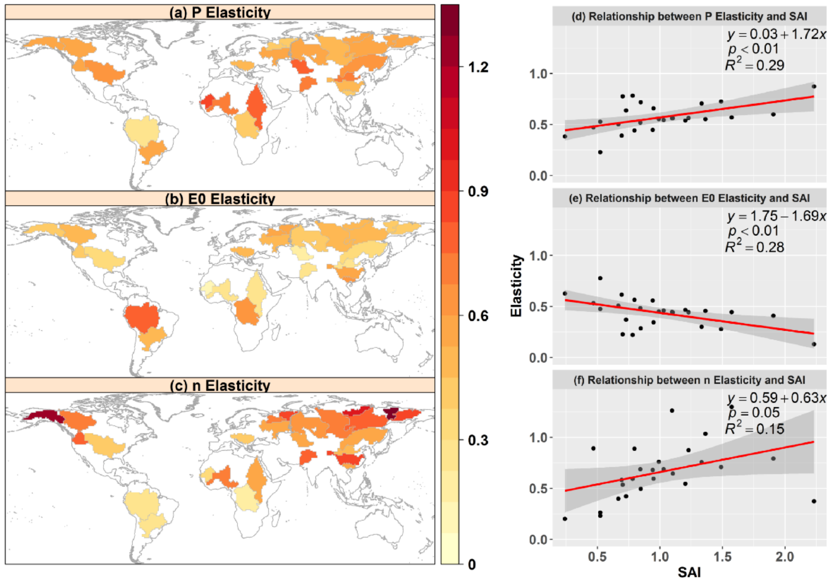

Figure 5. The climatic elasticity of evapotranspiration to the changing precipitation, potential evaporation and other factors represented by controlling parameter *n* in the 26 global large river basins, and its relations with the climate seasonality and asynchrony index (SAI). Noted that each point represents one of the 26 global large basins.

Hydrol. Earth Syst. Sci. Discuss., https://doi.org/10.5194/hess-2018-200
Manuscript under review for journal Hydrol. Earth Syst. Sci.
Discussion started: 23 April 2018

Hydrology and Earth System Sciences
Open Access
Discussions

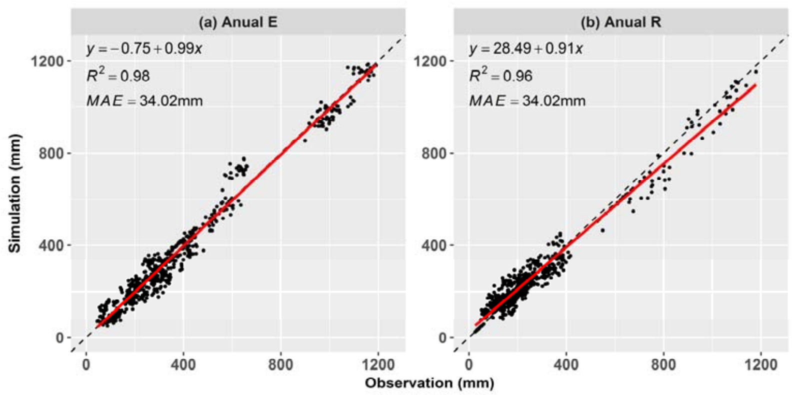

622
623 **Figure 6.** Simulation versus observation for (a) annual evapotranspiration and (b) annual runoff by using
624 Eq. (2) with the simulated parameter *n* regarding M and SAI as predictor using the semi-empirical formula
625 (i.e., eq. (14).

Hydrol. Earth Syst. Sci. Discuss., https://doi.org/10.5194/hess-2018-200
Manuscript under review for journal Hydrol. Earth Syst. Sci.
Discussion started: 23 April 2018

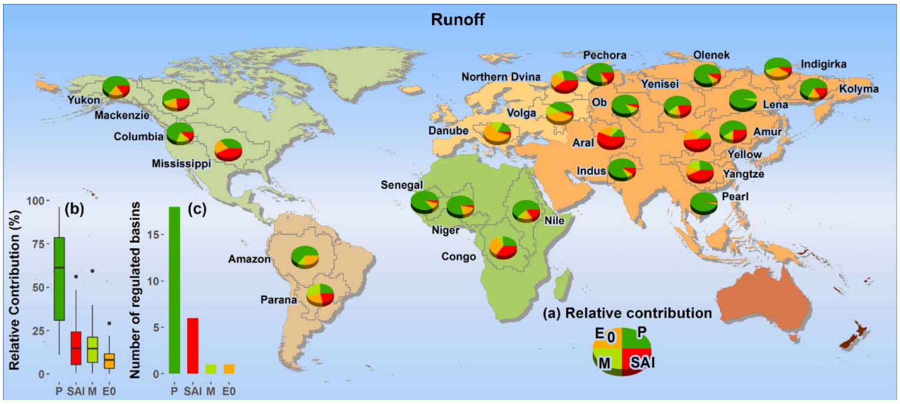

Figure 7. Relative contributions to the long-term mean changes of Runoff (before and after changepoint) from P_e), SAI, M and E_0 changes. The distribution ranges of relative contribution for each factor are shown in (b) and the number of basins dominated by each factor with the largest relative contribution is summarized in (c).

Hydrol. Earth Syst. Sci. Discuss., https://doi.org/10.5194/hess-2018-200
Manuscript under review for journal Hydrol. Earth Syst. Sci.
Discussion started: 23 April 2018

Hydrology and Earth System Sciences
Open Access
Discussions

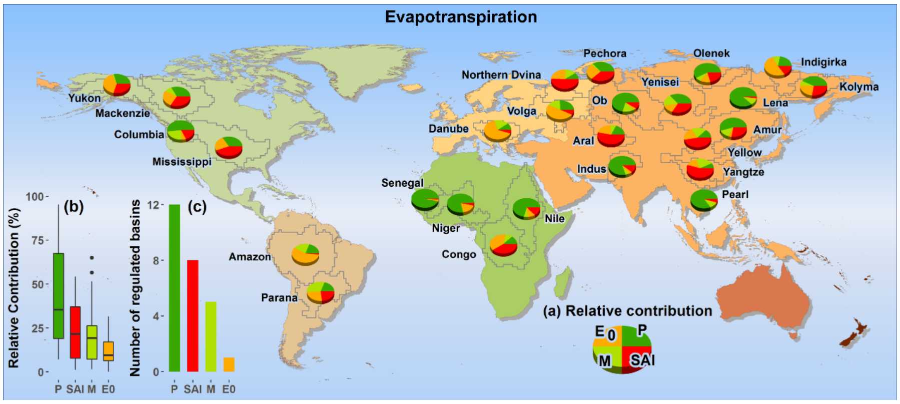

Figure 8. The same as Figure 7 but for relative contribution to the changes of evapotranspiration.